Phase and homodyne statistics of generalized squeezed states

Samuel L. Braunstein
Research House, 2639 East Fourth Street, Tucson, Arizona 85716-4417

Carlton M. Caves
Center for Laser Studies, University of Southern California, Los Angeles, California 90089-1112

(Received 18 May 1990)

We study the statistics of direct, heterodyne, and homodyne detection for some generalized squeezed states. The heterodyne statistics yield "classical" phase statistics, which give a clear picture of the phase-sensitive noise of these generalized squeezed states. The homodyne statistics display quantum-mechanical interference effects that are not present for ordinary squeezed states.

I. INTRODUCTION

Squeezed states[1] have been observed using homodyne detection, which allows one to measure the variance of a quadrature component of the incoming light field. Changes of this variance as the local-oscillator phase is varied yield a distinctive signature for squeezing. In this paper we investigate potential signatures for generalized squeezed states,[2–4] so called because they are generated from cubic, quartic, or higher-order interactions, which are the simplest generalizations of the quadratic interactions that generate ordinary squeezed states. For several examples of generalized squeezed states, we calculate the statistics of direct, heterodyne, and homodyne detection.

Fisher, Nieto, and Sandberg[2] initiated study of generalized squeezed states; they concluded that there is something seriously wrong with the evolution operators for all these interactions, after discovering that the vacuum-to-vacuum matrix elements of the evolution operators have divergent Taylor-series expansions in time. Braunstein and McLachlan[4] used techniques that improve the convergence of series expansions to perform numerical calculations for the cubic and quartic interactions; their results suggested that the Taylor expansions are actually asymptotic expansions of finite functions.

In this paper we consider again the cubic and quartic interactions, whose interaction Hamiltonians are given in the interaction picture by

$$\hat{H}_3 \equiv i\hbar\kappa(\hat{a}^{\dagger 3} - \hat{a}^3) , \tag{1}$$

$$\hat{H}_4 \equiv i\hbar\kappa(\hat{a}^{\dagger 4} - \hat{a}^4) . \tag{2}$$

Here $\hat{a}$ and $\hat{a}^\dagger$ are annihilation and creation operators for a single field mode, and κ is a generic coupling constant. In addition, we study a related interaction, introduced by Tombesi and Mecozzi,[5] whose interaction-picture interaction Hamiltonian is given by

$$\begin{aligned}\hat{H}_{2,2} &\equiv \hbar\kappa[i(\hat{a}^{\dagger 2} - \hat{a}^2)]^2 \\ &= -\hbar\kappa(\hat{a}^{\dagger 4} + \hat{a}^4) + \hbar\kappa(\hat{a}^{\dagger 2}\hat{a}^2 + \hat{a}^2\hat{a}^{\dagger 2}) .\end{aligned} \tag{3}$$

The interaction $\hat{H}_{2,2}$ has the interesting property that the vacuum-to-vacuum matrix element of its evolution operator can be written as a convergent integral, finite for all times, even though the matrix element has a zero radius of convergence when expanded as a Taylor series in time. Notice that the first term in $\hat{H}_{2,2}$ is identical to $\hat{H}_4$ under the rotation $\hat{a} \to \hat{a}e^{i\pi/8}$ and that the second term preserves photon number, so that its main effect is to modify phases.

II. GENERAL CONSIDERATIONS

The interaction-picture evolution operators for the three model Hamiltonians are given by

$$\hat{U}_3(r) = \exp[r(\hat{a}^{\dagger 3} - \hat{a}^3)] , \tag{4}$$

$$\hat{U}_4(r) = \exp[r(\hat{a}^{\dagger 4} - \hat{a}^4)] , \tag{5}$$

$$\hat{U}_{2,2}(r) = \exp[ir(\hat{a}^{\dagger 2} - \hat{a}^2)^2] , \tag{6}$$

where $r \equiv \kappa t$ is a scaled time.

The methods we use to perform calculations for the interactions $\hat{H}_3$ and $\hat{H}_4$ have been discussed elsewhere,[4] and the reader is referred there for details. The method[5] employed for $\hat{H}_{2,2}$ is of special interest, however, since it demonstrates how to obtain finite expressions for any matrix element of the evolution operator $\hat{U}_{2,2}(r)$. Tombesi and Mecozzi[5] noticed that $\hat{U}_{2,2}(r)$ may be written as a Gaussian average over the analytic continuation of a quadratic evolution operator:

$$\hat{U}_{2,2}(r) = \int_{-\infty}^{\infty} d\xi \frac{1}{\sqrt{\pi}} e^{-\xi^2} \exp[2\sqrt{ir}\xi(\hat{a}^{\dagger 2} - \hat{a}^2)] . \tag{7}$$

A matrix element of $\hat{U}_{2,2}(r)$ may thus be calculated in terms of the analytic continuation of the corresponding matrix element of a quadratic Hamiltonian. For instance, the vacuum-to-number-state matrix elements are given by

$$\langle n|\hat{U}_{2,2}(r)|0\rangle = \begin{cases} \left.\displaystyle\int_{-\infty}^{\infty} d\xi \frac{1}{\sqrt{\pi}} e^{-\xi^2} \frac{(\frac{1}{2}\tanh\tau)^{n/2}\sqrt{n!}}{\sqrt{\cosh\tau}\,(n/2)!}\right|_{\tau=4\sqrt{ir}\xi} & , n \text{ even} \\ 0, & n \text{ odd.} \end{cases} \tag{8}$$

In particular, the vacuum-to-vacuum matrix element can be written as the integral

$$\langle 0|\hat{U}_{2,2}(r)|0\rangle = \int_{-\infty}^{\infty} d\xi \frac{1}{\sqrt{\pi}} \frac{e^{-\xi^2}}{\sqrt{\cosh(4\sqrt{ir}\xi)}} . \tag{9}$$

When r is real, the denominator of the integrand in Eq. (9) is never zero, so the convergence of the integral rests solely on the integrand's behavior as $\xi \to \pm\infty$. The inequality $|\cosh z| \geq |\sinh \mathrm{Re}(z)|$ yields an upper bound on the integrand, which shows that the integral in Eq. (9) converges for real r.

Turn now to the convergence properties of the Taylor expansion about $r = 0$ of the vacuum-to-vacuum matrix element $\langle 0|\hat{U}_{2,2}(r)|0\rangle$. Taylor-series expansions converge within a radius—the radius of convergence—given by the first pole or branch point encountered in the complex plane. It is sufficient to study the pole structure of $\langle 0|\hat{U}_{2,2}(r)|0\rangle$ along the positive imaginary axis $r = i|r|$. Along this axis the denominator of the integrand in Eq. (9) becomes $\sqrt{\cos(4|r|^{1/2}\xi)}$, which has zeros whenever $4|r|^{1/2}\xi = \pi(l + \frac{1}{2})$, where l is any integer. The integration over ξ generates an accumulation of branch points right up to the origin along the $r = i|r|$ axis. Thus the Taylor expansion of $\langle 0|\hat{U}_{2,2}(r)|0\rangle$ has zero radius of convergence, even though $\langle 0|\hat{U}_{2,2}(r)|0\rangle$ is finite for real r, having been written in Eq. (9) as a convergent integral.

This behavior in the complex r plane is reminiscent of the accumulation of poles up to the origin seen numerically[4] for the vacuum-to-vacuum matrix elements of the evolution operators for the interactions $\hat{H}_3$ and $\hat{H}_4$. Indeed, the above analysis—together with the previous numerical work—gives us confidence that the model interactions $\hat{H}_3$, $\hat{H}_4$, and $\hat{H}_{2,2}$ are sensible generalizations of the ordinary quadratic squeezing interaction.

III. STATISTICS OF DIRECT, HETERODYNE, AND HOMODYNE DETECTION

We turn now to the statistics that would be observed in direct, heterodyne, and homodyne detection. For each kind of detection we neglect detection losses. The states we consider are generated from vacuum by the unitary evolution operators $\hat{U}_3(r)$, $\hat{U}_4(r)$, and $\hat{U}_{2,2}(r)$. Specifically, we present results for three states: (a) the state generated by $\hat{H}_3$ for scaled time $r = 0.5$, (b) the state generated by $\hat{H}_4$ for $r = 0.1$, and (c) the state generated by $\hat{H}_{2,2}$ for $r = 0.1$. We label these states generically by a density operator

$$\hat{\rho} = \hat{U}(r)|0\rangle\langle 0|\hat{U}^\dagger(r) . \tag{10}$$

In direct detection one counts the number of photons in the field mode of interest. The probability for counting n photons, called the photocount distribution, is given by

$$P_n = \langle n|\hat{\rho}|n\rangle , \tag{11}$$

where $|n\rangle$ is a photon-number eigenstate. Figure 1 shows the photocount distributions P_n for each of the three interactions. Not surprisingly, these plots show that $\hat{H}_3$ generates only photon triplets, while $\hat{H}_4$ and $\hat{H}_{2,2}$ generate only photon quadruplets. The tail in the photocount distribution for $\hat{U}_3(r)$ is quite long; the probabilities through $n = 18$ shown in Fig. 1(a) account for only 66% of the total probability. In contrast, the probabilities through $n = 20$ shown for $\hat{U}_4(r)$ and $\hat{U}_{2,2}(r)$ in Figs. 1(b) and 1(c) account for 93% and 97% of the total probability, respectively.

The Q function, defined by

$$Q(\alpha) \equiv \langle\alpha|\hat{\rho}|\alpha\rangle , \tag{12}$$

where $|\alpha\rangle$ is a coherent state, provides a normalized phase-space probability distribution, $Q(\alpha)/\pi$, for a quantum system. More than just a theoretical curiosity, $Q(\alpha)$ can be "measured" in a series of optimized simultaneous measurements of two orthogonal quadrature components[6] (that is, of two canonically conjugate variables like position and momentum), because $Q(\alpha)/\pi$ gives directly the statistics of such measurements. Applied to optical-frequency detection, this means that $Q(\alpha)/\pi$ gives the statistics of heterodyne detection,[7] which measures orthogonal quadrature components, or the statistics of a pair of homodyne detectors whose local oscillators have relative phases corresponding to measuring orthogonal quadrature components.[8] Furthermore, Eq. (12) is invertible,[9] so that $\hat{\rho}$ can be determined from $Q(\alpha)$.

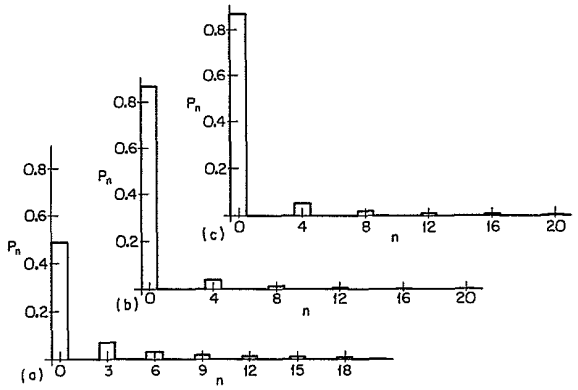

FIG. 1. Photocount distributions P_n, up to $n = 20$, for the states generated from vacuum by (a) $\hat{H}_3$ for time $r = 0.5$, (b) $\hat{H}_4$ for time $r = 0.1$, and (c) $\hat{H}_{2,2}$ for time $r = 0.1$.

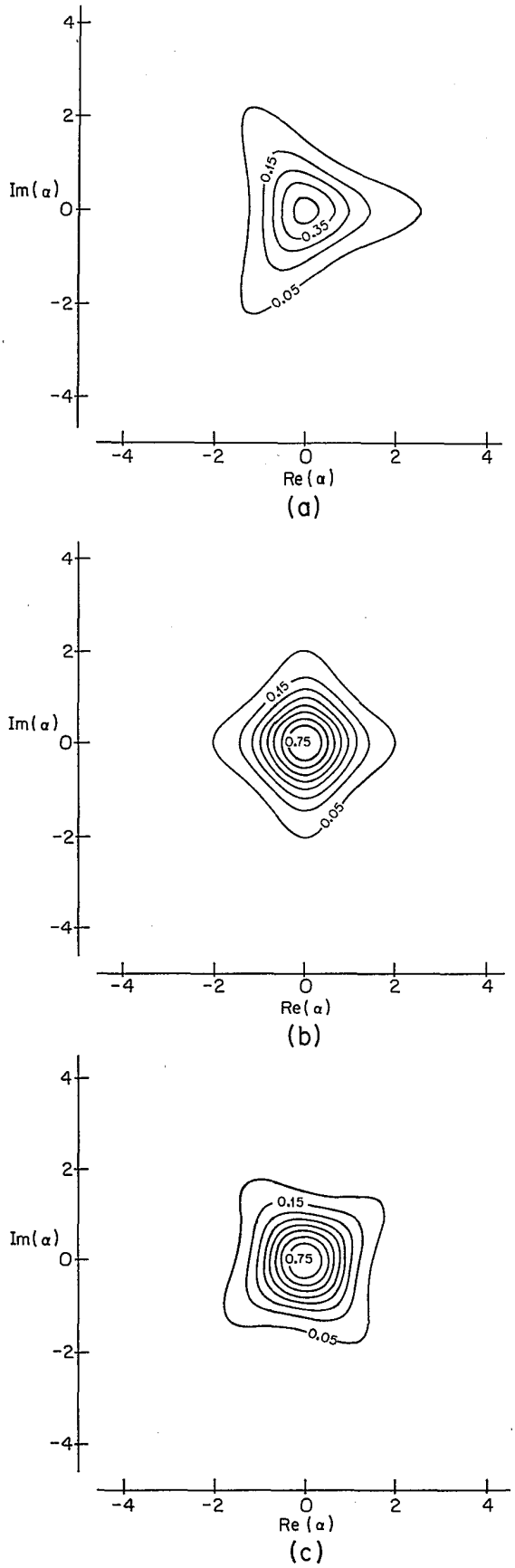

FIG. 2. Contour plots of the Q function $Q(\alpha)$ for the states generated from vacuum by (a) $\hat{H}_3$ for $r = 0.5$, (b) $\hat{H}_4$ for $r = 0.1$, and (c) $\hat{H}_{2,2}$ for $r = 0.1$.

In Fig. 2 we display contour plots of $Q(\alpha)$ for the states generated by each of the three interactions. Braunstein and McLachlan[4] have given previously contour plots of the Q function for states generated by $\hat{H}_3$ and $\hat{H}_4$; those cases are included here for completeness. Notice the similarity between the Q functions generated by $\hat{H}_4$ and $\hat{H}_{2,2}$: the Q function generated by $\hat{H}_{2,2}$ [Fig. 2(c)] is nearly the same as that generated by $\hat{H}_4$ [Fig. 2(b)], except for a counterclockwise rotation of about 37°. Since the first term of $\hat{H}_{2,2}$ accounts for a 22.5° rotation, the remaining rotation must come from the second term in $\hat{H}_{2,2}$ (Q-function plots for smaller values of r confirm this supposition). Though this similarity is not surprising, it does support the numerical results of Braunstein and McLachlan.[4] Figure 3 shows a three-dimensional rendering of the Q function for the state generated by $\hat{H}_3$, the same state whose contour plot appears in Fig. 2(a); the three-dimensional view shows clearly the scale of the "arms."

As emphasized by Shapiro and Wagner,[7] the results of heterodyne detection determine a phase θ for the detected mode, where θ is defined relative to a phase reference supplied by the local oscillator. The (normalized) probability distribution of θ is obtained by integrating $Q(\alpha)/\pi$ along "wedges" extending from the origin:

$$P(\theta) = \int_0^\infty |\alpha|\, d|\alpha| \frac{Q(\alpha)}{\pi} , \tag{13}$$

Such a measurement of phase is effectively a "classical" measurement, since the Q function applies to simultaneous measurement of two noncommuting observables, a process that inevitably introduces additional noise.[6,10,11]

Schleich, Horowicz, and Varro[12] use an abstract phase probability distribution—the probability density that the mode occupies a phase "eigenstate"—to demonstrate that ordinary squeezed vacuum has two well-defined

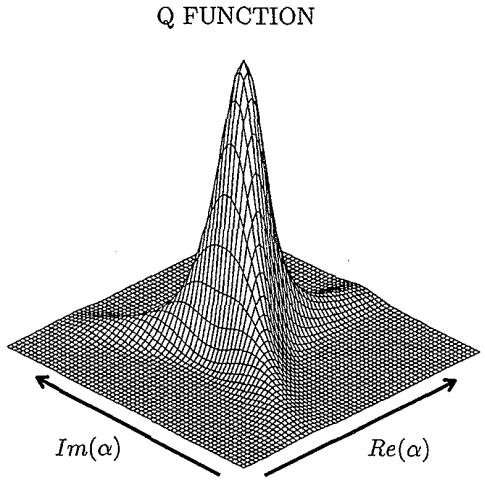

FIG. 3. Three-dimensional plot of the Q function $Q(\alpha)$ for the state generated from vacuum by $\hat{H}_3$ for $r = 0.5$. This three-dimensional view draws attention to the scale of the arms.

peaks in phase, 180° apart, and further that these peaks merge into a single peak when the state is displaced along the axis of reduced fluctuations. It is not clear how to measure the phase probability distribution they discuss; in contrast, the phase probability distribution (13) shows the same effect for ordinary squeezed vacuum and can be achieved experimentally.[8]

In Fig. 4 we plot $P(\theta)$ for the states generated by the three interactions. Clearly, the three- and four-peaked structures are inherited from the "arms" of the corresponding Q functions exhibited in Fig. 2. To calculate these phase distributions we integrated the Q functions out to $|\alpha| = 5$. This leaves $P(\theta)$ for the state generated by $\hat{H}_3$ normalized to 0.66, since a large portion of $Q(\alpha)$ for this state lies outside the integration region in phase space [see Fig. 2(a)]. Similarly, the phase distributions for $\hat{H}_4$ and $\hat{H}_{2,2}$ are normalized to 0.93 and 0.97, respectively. Notice that the phase distribution for the state generated by $\hat{H}_{2,2}$ [Fig. 4(c)] is slightly asymmetric about its maxima and minima.

Homodyne detection measures a quadrature component

$$\hat{x}_\theta \equiv \tfrac{1}{2}(\hat{a}e^{-i\theta} + \hat{a}^\dagger e^{i\theta}) , \tag{14}$$

where θ is a phase determined by the phase of the local oscillator. The statistics of homodyne detection—that is, the probability distribution $P(x_\theta)$ of the quadrature component—are given by the diagonal matrix elements of the density operator in the x_θ basis (for a pure state, the absolute square of the x_θ wave function) or, alternatively, in terms of the (normalized) Wigner function $W(x_\theta, p_\theta)$ for orthogonal quadrature components x_θ and p_θ:

$$P(x_\theta) = \langle x_\theta|\hat{\rho}|x_\theta\rangle = \int dp_\theta\, W(x_\theta, p_\theta) . \tag{15}$$

Here $|x_\theta\rangle$ denotes an eigenstate of $\hat{x}_\theta$. The homodyne statistics correspond to projecting the Wigner quasiprobability distribution onto the x_θ axis.[13] Coherent pieces of the distribution which are projected onto the same interval of the x_θ axis interfere with each other, giving rise to a fringe pattern with a local fringe spacing varying inversely as the phase-space distance between the interfering pieces.

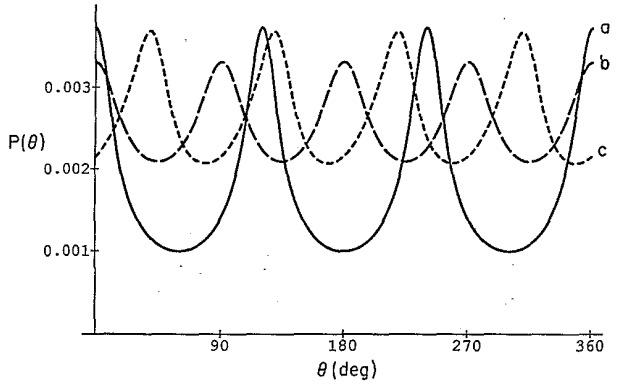

FIG. 4. "Classical" phase distributions $P(\theta)$ for the states generated from vacuum by (a) $\hat{H}_3$ for $r = 0.5$ (solid line), (b) $\hat{H}_4$ for $r = 0.1$ (long-dashed line), and (c) $\hat{H}_{2,2}$ for $r = 0.1$ (short-dashed line).

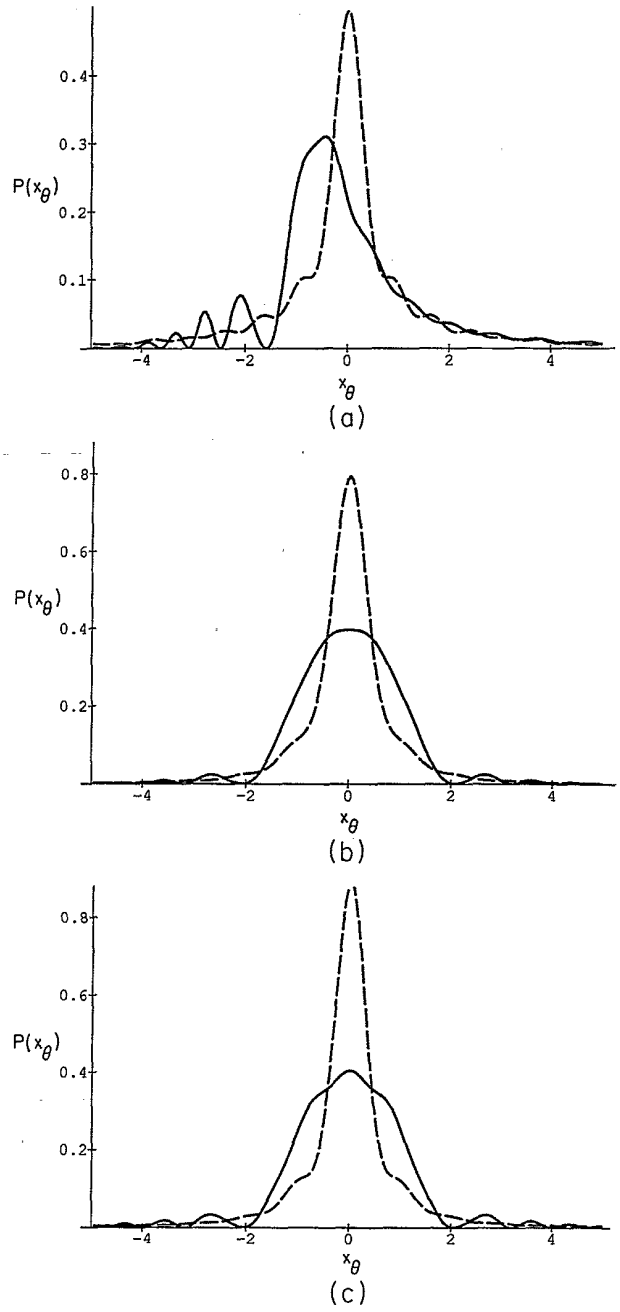

FIG. 5. Homodyne probability distributions $P(x_\theta)$ for the states generated from vacuum by (a) $\hat{H}_3$ for $r = 0.5$, with local-oscillator phases $\theta = 0°$ (solid line) and $\theta = 90°$ (dashed line); (b) $\hat{H}_4$ for $r = 0.1$, with $\theta = 45°$ (solid line) and $\theta = 0°$ (dashed line); and (c) $\hat{H}_{2,2}$ for $r = 0.1$, with $\theta = 80.5°$ (solid line) and $\theta = 37.5°$ (dashed line). The angles for $\hat{H}_{2,2}$ (80.5° and 37.5°) are determined from the minima and maxima of the corresponding phase distribution displayed in Fig. 4(c); due to the slight asymmetry in this phase distribution the two angles are not 45° apart.

Although the homodyne statistics are rigorously a projection of the Wigner distribution, it is possible to visualize these statistics in terms of the projection of some other quasiprobability distribution, such as the Q functions displayed in Fig. 2. As an example,[13,14] consider a superposition of coherent states given by $2^{-1/2}(|\beta\rangle + |-\beta\rangle)$. As long as $|\beta|$ is greater than about 2, the Q function for this state is very nearly half the sum of the Q functions for two separate coherent states $|\beta\rangle$ and $|-\beta\rangle$. The homodyne statistics depend on the phase of the local oscillator. When this phase corresponds to projecting the two coherent states on top of one another, fringes with a spacing of $\pi/2|\beta|$ appear within an envelope given by the probability distribution $P(x_\theta)$ for the vacuum state. Shifting the phase of the local oscillator by 90° corresponds to a projection orthogonal to the one just described; the probability distribution $P(x_\theta)$ is then very nearly half the sum of the separate distributions for coherent states at $|\beta|$ and $-|\beta|$.

In our discussion of generation, we ignore losses, so the states we consider are pure states. Thus the "arms" in each contour plot of Fig. 2 are coherent with each other, and we expect to see interference between the arms in the homodyne statistics, when the local oscillator phase is chosen appropriately. For example, Fig. 5(a) displays homodyne probability distributions $P(x_\theta)$ for the state generated from vacuum by $\hat{U}_3(r)$ for $r = 0.5$, the same state whose Q-function contours are plotted in Fig. 2(a). The solid line in Fig. 5(a) shows the homodyne statistics for $\theta = 0°$ (projection onto the real axis); there are quite obvious interference fringes on the left side of the origin, but only faint wiggles on the right. A glance back at Fig. 2(a) suggests that the interference fringes on the left side are a result of interference between the two arms at 120° and 240°, while the behavior on the right is—aside from the faint wiggles—what one would expect from projection of the single arm at 0°. We have not been able to interpret the faint wiggles on the right side in terms of projection of the Q function. The dashed line in Fig. 5(a) displays the homodyne probability distribution for the same state for $\theta = 90°$ (projection onto the imaginary axis); there is a narrow central peak with long tails on each side. The narrow central peak comes from the projection of the Q-function arm at 0°, and the tails arise from projection of the arms at 120° and 240°. Again the low contrast wiggles are not easily understood. The main features seen in the other parts of Fig. 5 can be interpreted in a similar way.

IV. CONCLUSION

We have studied the statistics of direct, heterodyne, and homodyne detection for generalized squeezed states generated from vacuum by the interactions $\hat{H}_3$, $\hat{H}_4$, and $\hat{H}_{2,2}$. The homodyne statistics display quantum-mechanical interference effects, while the heterodyne statistics are described by an essentially "classical" phase-space distribution $Q(\alpha)/\pi$, classical because of the noise introduced by measuring canonically conjugate observables.[6,10,11] As a consequence, the features displayed by the heterodyne statistics [for example, the multipeaked phase probability distributions $P(\theta)$ in Fig. 4] are likely to be more robust in the presence of noise and losses than are the intrinsically quantum-mechanical effects exhibited in the homodyne statistics. By the same token, however, the features of the heterodyne statistics can be more easily mimicked by classical states, such as an incoherent superposition of coherent states, so a clear-cut signature for generalized squeezed states is likely to require detection of the quantum-mechanical features exhibited by the homodyne statistics.

ACKNOWLEDGMENTS

This work was supported in part by an AT&T Research contract at the University of Southern California.

[1]For reviews of squeezed states, see R. Loudon and P. L. Knight, J. Mod. Opt. **34**, 709 (1987); M. C. Teich and B. E. A. Saleh, Quantum Opt. **1**, 153 (1989).
[2]R. A. Fisher, M. M. Nieto, and V. D. Sandberg, Phys. Rev. D **29**, 1107 (1984).
[3]M. Hillery, M. S. Zubairy, and K. Wodkiewicz, Phys. Lett. A **103**, 259 (1984).
[4]S. L. Braunstein and R. I. McLachlan, Phys. Rev. A **35**, 1659 (1987).
[5]P. Tombesi and A. Mecozzi, Phys. Rev. A **37**, 4778 (1988).
[6]E. Arthurs and J. L. Kelly, Jr., Bell. Syst. Tech. J. **44**, 725 (1965).
[7]J. H. Shapiro and S. S. Wagner, IEEE J. Quantum Electron. **QE-20**, 803 (1984).
[8]N. G. Walker and J. E. Carroll, Opt. Quant. Electron. **18**, 355 (1986).
[9]W. H. Louisell, *Quantum Statistical Properties of Radiation* (Wiley, New York, 1973).
[10]Y. Yamamoto and H. A. Haus, Rev. Mod. Phys. **58**, 1001 (1986).
[11]E. Arthurs and M. S. Goodman, Phys. Rev. Lett. **60**, 2447 (1988).
[12]W. Schleich, R. J. Horowicz, and S. Varro, Phys. Rev. A **40**, 7405 (1989).
[13]K. Vogel and H. Risken, Phys. Rev. A **40**, 2847 (1989).
[14]B. Yurke and D. Stoler, Phys. Rev. Lett. **57**, 13 (1986).